Catalysis Science & Technology

ROYAL SOCIETY OF CHEMISTRY

PAPER

View Article Online
View Journal | View Issue

Cite this: *Catal. Sci. Technol.*, 2022, 12, 5349

Mechanistic insights into the CO_2 capture and reduction on K-promoted Cu/Al_2O_3 by spatiotemporal *operando* methodologies†

Donato Pinto, Victor van der Bom Estadella and Atsushi Urakawa *

Integrated CO_2 capture and conversion processes bring the promise of drastic abatement of CO_2 emission together with its valorisation to chemical building blocks such as CH_4 and CO. Isothermal CO_2 capture and reduction (CCR) on a K-promoted Cu/Al_2O_3 was recognised as an effective catalytic strategy for removing CO_2 from diluted stream and converting it to syngas (H_2 + CO) employing green H_2 as reducing agent. The dual functionality of the catalyst is the key of this dynamic process, in which the alkaline metal introduces the capture functionality and copper ensures the selective conversion of the captured CO_2 to CO. However, the highly dynamic state of the catalyst at reaction conditions represents a barrier for the identification of the catalytic mechanism of CCR, which is vital for rational process improvement and design. In this work, we conducted a mechanistic investigation of CCR by means of spatiotemporal *operando* methodologies, gaining insights into dynamic variation of temperature, gas concentration and reactive surface species in the CCR reactor. The results show the unique potassium state exothermically captures CO_2 as surface carbonates which can be reduced to CO rapidly under H_2 atmosphere. When the surface carbonates are transformed to formates the reaction path is altered and the reduction to CO becomes slower. By designing controlled catalytic experiments, we further demonstrate the active involvement of CO in the capture mechanism and the effectiveness of CO_2 capture in presence of an oxidised surface, extending the perspectives and suitability of CCR to treat actual complex effluent streams.

Received 31st January 2022,
Accepted 15th July 2022

DOI: 10.1039/d2cy00228k

rsc.li/catalysis

Introduction

The urgency of reducing anthropogenic emissions of CO_2 has given impulse to the elaboration of carbon capture and utilisation (CCU) strategies. Such strategies are designed to substantially reduce the CO_2 emissions of industrial processes and power plants by separating CO_2 from exhaust gases and, after purification and compression, making it available as feedstock for chemicals and fuels production. Compared to the alternative carbon capture and storage (CCS) that treat CO_2 as a waste, CCU technologies extract value from the captured CO_2 by employing it as a carbon source to produce carbon-neutral commodities.[1–4]

Several technological options have been investigated and developed for CO_2 capture, including amine-based liquid solutions, solid sorbents, separation membranes, ionic liquids, cryogenic separation and biological systems among others.[5–8] Technologies employing amine-based solutions, in particular monoethanolamine, are available at commercial stage, although their employment put some constraints on the capture process.[9] The flue gases containing CO_2 need to be cooled down to an optimal temperature of operation, which is around 40–60 °C for amines. Moreover, O_2, dust, NO_x and SO_x compounds often have to be separated from the flue gas, since they act as poisoning agent provoking the decomposition of the solvent. After saturation of the solution with CO_2, an energy-intensive CO_2 desorption and solvent regeneration has to be performed.

Solid sorbents, including metal oxides, zeolites, carbon, polymers and metal organic frameworks, partially overcome the constraints introduced by an absorbent in the liquid phase, with great promises to reduce capital costs and energy requirements for regeneration.[10–12] Alkaline metal oxides, especially CaO, present high affinity towards CO_2 capture and are tested in carbonation cycles.[13] However, their thermal regeneration requires high temperatures, leading to particle sintering and capture efficiency losses.

Despite the promising readiness of the available technologies, the operational costs related to CO_2 capture still represent the main limitation. Such costs become prohibitive to capture diluted CO_2, as in the case of flue gases

Catalysis Engineering, Department of Chemical Engineering, Van der Maasweg 9, 2629 HZ, Delft, The Netherlands. E-mail: A.Urakawa@tudelft.nl

† Electronic supplementary information (ESI) available. See DOI: https://doi.org/10.1039/d2cy00228k

emitted by power plants, cement and steel industry, in which the capture cost can exceed 100 USD per ton of CO_2.[14] Furthermore, high purity CO_2 needs to be separated and compressed to be sourced to the chemical industry. The current CO_2 utilisation involves mainly urea synthesis and other small-scale applications (food industry, methanol, carboxylic acids synthesis, *etc.*), that accounts for transforming an amount of CO_2 equivalent to 0.5% of its annual emissions.[15,16] Consequently, it is more desirable to design processes which can directly and successfully handle diluted sources of CO_2, as flue gases from power plants, or even make use of the hundreds of ppm concentration in air, in order to reduce the costs related to purification and compression steps.

Anticipating wider availability of economic green H_2 in the near future, the combination of CO_2 capture with its direct conversion to more appealing carbon-containing molecules, can bring additional value to the product.

In the last decade, several research groups have proposed and demonstrated integrated CO_2 capture and conversion processes.[17,18] By using a properly functionalized solid catalyst, CO_2 from diluted streams is captured and stored in the material. Successively, employing H_2 as a reducing agent, the captured CO_2 can be selectively converted to more appealing carbon-containing molecules like CO and CH_4 with a wider range of applications in chemical industry than CO_2. With economic green H_2 availability, such processes will become competitive options to close the carbon-cycle.

Farrauto and coworkers[19] proved the feasibility of the concept by means of a bifunctional catalyst, in which a combination of alkaline metal oxide (CaO) and transition metal (Ru) supported on γ-Al_2O_3 provided efficient capture of CO_2 from diluted streams and its subsequent conversion to CH_4 when the atmosphere was switched to H_2. A key characteristic of the process is that both capture and conversion steps can take place at the same pressure and in isothermal conditions. Thanks to the nanodispersion of the alkali component on the support, the regeneration of the sorbent in H_2 was achieved at temperatures as low as ~300 °C, permitting to reduce the energy requirements compared to the case of bulk CaO regeneration. A similar integrated process, referred to as CO_2 capture and reduction (CCR), was demonstrated by our research group employing catalysts containing abundant chemical elements.[20] Potassium was introduced as efficient promoter for CO_2 sorption, while the combination of Fe, Cu and Cr exhibited high performance targeting the selective formation of CO, in view of obtaining a valuable syngas mixture (H_2 + CO) in the product stream.

The interest in the catalytic process has grown recently with the exploration of alternative catalytic formulations. Several alkali (Li, Na, K, Cs) and alkali earth promoters (Ca, Ba) can be employed to introduce the CO_2 capture functionality.[21–24] The conversion of the captured CO_2 is selectively driven towards the desired product by proper selection of the active metal phase. In particular, Cu-based catalysts exhibited selective reduction to CO,[20,25] while Ru and Ni were employed for methanation.[26–29]

Recently, Kosaka *et al.*[30] demonstrated the beneficial effect of increasing reaction pressures (up to 9 bar) to enhance the performances of direct CO_2 capture at the level of the atmosphere and CH_4 formation on a Na-promoted Ni/Al_2O_3 catalyst.

Despite a trending research directed towards optimisation of CCR processes, knowledge regarding the fundamental catalytic mechanism is still limited. *Ex situ* investigation of the catalytic materials inherently lacks information about the active catalytic state. Hyakutake *et al.*[25] employed a K-promoted Cu/Al_2O_3 catalyst as model systems to investigate the peculiar characteristics of the active phase for CO_2 capture and reduction. *Operando* diffuse reflectance infrared Fourier transform spectroscopy (DRIFTS) suggested the formation of surface intermediates assigned to formates on potassium, while *operando* XRD analysis revealed a highly dynamic system in reaction conditions, with a complex state composed of an highly amorphous potassium state and nanodispersed copper. At the operation temperatures, the dynamic nature of the catalytic system varies in time and space, requiring spatiotemporal analytical techniques to elucidate the CCR chemistry and to identify the catalytic roles played by the K and Cu phases.

In this contribution, we aimed to deepen the comprehension on the catalytic mechanism responsible for CO_2 capture and reduction on a K-promoted Cu/Al_2O_3 system, by identifying active reaction paths of the CCR catalysis. Spatiotemporal sampling of temperature and gas composition along the catalytic bed were used, while *operando* DRIFTS was used to identify spatiotemporal variations of reactive surface species. Unprecedented mechanistic insights were gained by the substitution of CO_2 with CO at the inlet stream and from the evaluation of how CCR operates when Cu is oxidised.

Results and discussion

A Cu–K/γ-Al_2O_3 catalyst (11 wt% Cu, 10 wt% K) was synthesised by a two-step incipient wetness impregnation method, following the procedure already reported for similar materials.[25] The successful outcome of the synthesis was verified by X-ray diffraction (Fig. S1†).

Fig. 1 shows a representative concentration profile during the CCR catalytic test performed at 350 °C on the Cu–K/γ-Al_2O_3 catalyst.

In a typical CCR catalytic test, 0.25 g of catalyst are first activated by exposure to a reducing stream at 450 °C (100% H_2, 50 mL min^{-1}, 1 h). During this pretreatment, CuO is fully reduced to metallic Cu, while the highly dispersed K_2CO_3 phase is partially decomposed. The presence of copper enhances the decomposition of K_2CO_3 at lower temperature compared to bulk K_2CO_3 or K/Al_2O_3 system, as confirmed by TGA analysis (Fig. S3†). As a result, active sites for the capture of CO_2 are generated. Then, the catalyst is cyclically exposed to the alternating reactive gases. First, a CO_2 feed (10% in He, 15 mL min^{-1}) is passed to the catalyst bed, from which

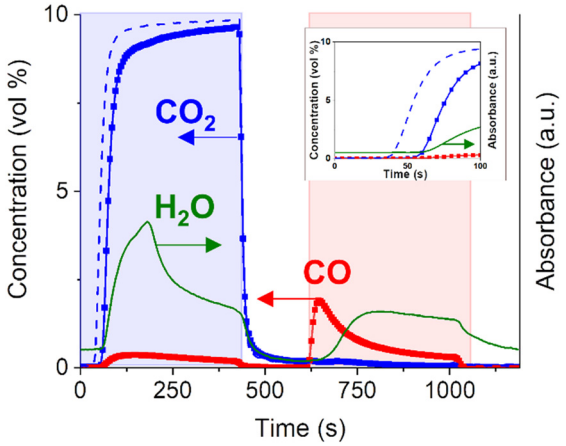

Fig. 1 Outlet gas concentrations during CCR performed at 350 °C. 1 CCR cycle consists of CO_2 feed (0–420 s, 15 mL min^{-1}, 10% in He), inert flush (420–595 s, 30 mL min^{-1}, He), H_2 (595–1015 s, 15 mL min^{-1}, 100%), inert flush (1015–1190 s, 30 mL min^{-1}, He) and the cycle is repeated. Results are averaged over 18 CCR cycles. CO_2 blank signal (dotted line) obtained as average of 2 CCR cycles during blank experiment at room temperature. The inset shows the concentration profiles during the initial phase of the CO_2 capture phase (0–100 s).

CO_2 is captured until saturation of the active sites. For this catalytic test (Fig. 1), an excess of CO_2, compared to the CO_2 capture capacity of the catalyst, is passed to the reactor in order to study the reaction paths before and after catalyst saturation. It is possible to maximize the full CO_2 capture period by adjusting gas flow rate, catalyst amount and CO_2 concentration. An inert flush phase (He, 30 mL min^{-1}) is then introduced to the reactor to remove weakly-adsorbed species and avoid mixing of reactants and related gas-phase reactions for more precise mechanistic studies. After that, H_2 is introduced to the reactor (100%, 15 mL min^{-1}) to remove the adsorbed CO_2 in the form of CO and regenerate the catalytically active phase, followed by an additional inert flush phase (He, 30 mL min^{-1}). Fig. 1 reports the average of the cycles with stable catalytic activity achieved after the first non-reproducible cycle. Compared to the CO_2 profile obtained for a blank experiment performed on the inactive catalyst bed at room temperature, the delay in the appearance of CO_2 at the outlet (20 s) suggests that CO_2 is aggressively captured by the catalyst. Quantitative evaluation of the outlet stream composition clarifies that *ca.* 100% of CO_2 was captured during this initial period. No CO signal is detected in this time interval within the detection limit (*ca.* 100 ppm), resulting in virtually a CO_x-free reactor effluent.

Once saturation of the capture sites is achieved, most of the CO_2 entering the reactor is directly released to the reactor outlet apart from a small fraction reacting to produce CO. The detection of CO only after the end of the initial active capture period suggests that the active sites generated on this catalyst may be active for both CO_2 and CO capture. Interestingly, the outlet gas analysis (Fig. 1) highlighted the formation of water during the capture phase. The formation of water in the CO_2 atmosphere indicates the presence of active H or OH species, generated during catalyst exposure to gaseous H_2 and stored on the catalyst surface. The identification of such species seems directly related to the catalytically active phase and will be targeted in the following sections.

Upon switching to the reduction (H_2) feed, the captured CO_2 is instantaneously and selectively reduced to CO and no other carbon-containing products such as CH_4 are observed within the detection limit (Fig. 1). The sharp peak of CO detected at the outlet is not accompanied by water formation. The water signal starts to rise with a significant delay (*ca.* 60 s) compared to the start of the H_2 phase (595 s). This excludes a direct correlation of water formation to the main reduction mechanism of captured CO_2 towards CO formation.

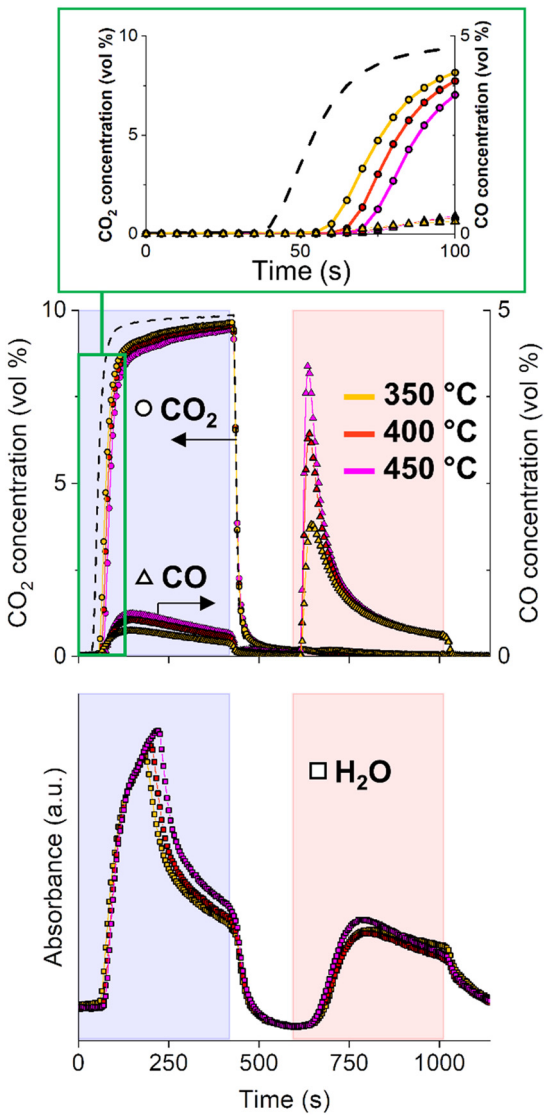

Fig. 2 Outlet gas concentrations of CO_2 (○) and CO (△) and signal of H_2O (□) during CCR performed at 350 °C (yellow profiles), 400 °C (red profiles), 450 °C (magenta profiles). Results are averaged of 18 CCR cycles. CO_2 blank signal (dotted line) obtained as average of 2 CCR cycles during blank experiment at room temperature.

The presence of unconverted H_2 and CO in the effluent stream generates a syngas, whose quality, after separation of water in the product stream, is generally defined by the H_2/CO ratio. The beauty of the CCR is the flexibility of the process, since this ratio can be tuned by the H_2 flow rate, the reduction period, the reduction rate defined by the catalyst and also the reaction temperature.

Effect of reaction temperature

In general, reaction temperature is one of the process parameters greatly affecting CCR performance. Fig. 2 compares the CCR activity at three different temperatures, namely 350, 400 and 450 °C. At higher temperatures, the CO_2 is detected in the reactor effluent during the capture phase increasingly delayed, revealing an higher capture capacity of the material. Increasing the temperature is beneficial for the CCR reaction. At higher temperature, a larger portion of potassium active sites for capture is likely regenerated in H_2 atmosphere at each cycle. This is in line with the increased weight loss detected at 450 °C during H_2-TGA, which is related to decomposition of the potassium phase (Fig. S2†). As a consequence, the amount of CO_2 removed from the feed gas increases from 54 μmol g_{cat}^{-1} (350 °C), 95 μmol g_{cat}^{-1} (400 °C) to 130 μmol g_{cat}^{-1} (450 °C).

After the initial active capture, the amount of CO produced by direct interaction of CO_2 with the catalyst slightly increases with temperature. Some considerations can be made from the qualitative analysis of the water signals evolved during the CO_2 stream at different temperatures. On the one hand, the slight increase in water signal with temperature, associated to the increased amount of CO formation, indicates that a CO_2 hydrogenation path to CO is active, which is enhanced at higher temperatures in accordance with the endothermic RWGS reaction.[31] As mentioned earlier, CO is only detected after saturation of the capture sites, when the CO_2 signal starts to rise. The initial absence of CO detection suggests that CO has affinity towards the capture sites and may directly participate in the capture mechanism.

The analysis of the gaseous species at the reactor outlet permits to identify three main reactions taking place during the CO_2 capture phase:

$$CO_2 + \square = CO_{2(a)} + H_2O \quad (1)$$

$$CO_2 + 2H_{(a)} = CO + H_2O \quad (2)$$

$$CO + \square = CO_{(a)} \quad (3)$$

where (□) represent an active sites for CO_x capture on the catalyst. $CO_{2(a)}$ and $CO_{(a)}$ do not necessarily indicate simple adsorbed states of the respective molecules, but rather molecules trapped in the form of surface/bulk chemical species like carbonate. Determining the type of adsorbed species formed during CO_x capture is crucial to identify the active sites for CCR and such studies are described in the following sections.

When the feed gas is switched to H_2, the comparison of the catalytic activity profiles at different temperatures clarifies the presence of two distinct mechanisms involved in the formation of CO.

The first mechanism is associated with the initial fast release of CO. At higher temperatures, the peak of CO reaches higher values, consistent with the higher amount of CO_2 captured. Interestingly, this initial CO release is not accompanied by any water formation (*vide supra*). The absence of a marked release of water at this stage suggests the absence of CuO formation during the CO_2 capture stage, as evidenced in a previous work.[25] This also excludes the relevance of a redox reaction involving a Cu/Cu_xO cycle as mechanism for CO_2 reduction for this catalytic system. Rather, CO_2 is reduced by active H species formed by H_2 dissociation on Cu (reaction (4)). However, this reaction does not follow a standard hydrogenation path (RWGS, reaction (5)) leading to CO and water release as a consequence of CO_2 reduction. Rather, during the initial reduction phase of CCR, the excess of active H species generated in the reduction phase may induce the destabilisation of the surface intermediates formed during CO_2 capture, provoking the fast selective release of CO (reactions (6) and (7)). Results from the investigation of surface species and their dynamics in capture and reduction phases are fundamental to elucidate the type of mechanism involved.

$$H_2 = 2H_{(a)} \quad (4)$$

$$CO_{2(a)} + H_2 = CO + H_2O \quad (5)$$

$$CO_{2(a)} + 1/2H_2 = OH_{(a)} + CO \quad (6)$$

$$CO_{(a)} + 1/2H_2 = H_{(a)} + CO \quad (7)$$

After the fast initial release, a second mechanism is responsible for the long tailing in the CO signal. This slowly decaying CO signal seems to be correlated with the water signal. Interestingly, both CO and water profiles deriving from this mechanism are not affected by change in reaction temperature. This contrasts with the hypothesis of a reverse water-gas shift type of reaction which would in turn be favoured at higher temperatures. Mass transfer limitations generated in the packed bed reactor, as well as the presence of less active catalytic sites may be responsible for this reaction. However, the analysis of the outlet stream composition lacks of spatial resolution to answer the question.

Spatiotemporal *operando* studies of temperature, concentration and surface species in the reactor

The analysis of the catalytic activity profiles characterised by the outlet stream concentrations offers relevant indications

on the type of reactions involved in CCR. However, the information retrieved at the reactor outlet lacks spatial resolution, potentially missing any temperature or concentration gradients developed in the reactor bed. Moreover, such results are detached from any consideration on the catalyst state and dynamic of surface species involved in the capture of CO_2 and selective conversion to CO. In particular for the Cu–K/Al_2O_3 system, the unique catalytic state reached in operation conditions does not permit to make conclusive statements based on *ex situ* data.[25] To obtain deeper understanding of the reaction mechanisms involved in CCR, we performed *operando* spatiotemporal sampling of temperature and gas concentration along the reactor bed. In addition, with the aim of identifying the surface reaction mechanisms involved in the CCR reaction, we performed spatiotemporal *operando* DRIFTS and compared the dynamics of surface species with the evolution of the catalytic activity.

Fig. 3 contains the results obtained from spatiotemporal sampling of concentration and temperature by means of a moving capillary system under CCR with Cu–K/γ-Al_2O_3 at 350 °C. The reaction condition employed was identical to that of the experiment shown in Fig. 1. A schematic of the sampling positions is represented in Fig. 3A. The sampling positions inside the bed are indicated with the relative position, where positions 0 and 1 correspond to quartz wool at the front and

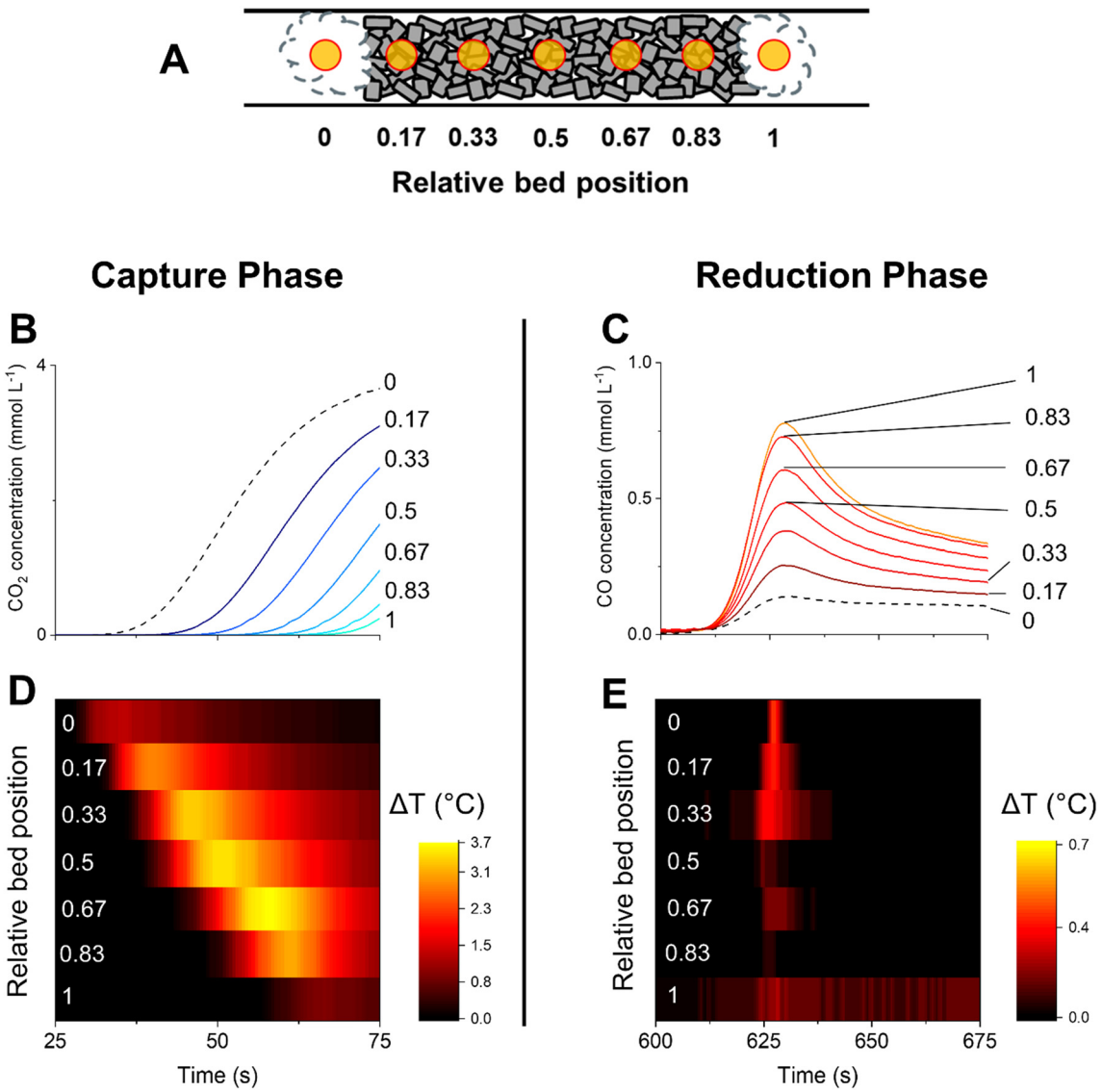

Fig. 3 Spatiotemporal profiling of temperature and gas phase composition (MS) along the catalyst bed during CCR at 350 °C. Schematic of different sampling positions (A) shown in the relative position (0: beginning of the catalyst bed, 1: end of the catalyst bed). Position 0 and 1 correspond to quartz wool at the front and after the catalyst bed, respectively. CO_2 (B) and CO (C) concentration profiles obtained for the initial stage of the capture phase and reduction phase, respectively. Dashed black line correspond to the signal collected at position 0 in the quartz wool in front of the bed. Temperature of the catalyst bed sampled at different positions from the front to the end of the catalyst bed during the initial stage of the capture phase (D) and reduction phase (E).

after the catalyst bed, respectively. Fig. 3B highlights the evolution of CO_2 sampled at different positions along the catalyst bed during the initial stages of the capture phase and analysed by mass spectrometry. Moving along the bed (relative position from 0 to 1), the CO_2 is detected at progressively increasing times, confirming the existence of an active adsorption front proceeding until saturation of the active sites at each position.

At the same time, a temperature increase is detected before the detection of gaseous CO_2 at each position (Fig. 3D *vs.* B). The capture is then associated with an exothermic process which can result from the adsorption of CO_2 from the gas phase. This is consistent with the exothermic reaction of CO_2 with K_2O or KOH to form carbonate or bicarbonate species (reactions (8)–(11)).[32] However, the generation of water during the capture reaction suggests that the mechanism of CO_2 capture may involve a potassium hydroxide phase with formation of carbonates species (reaction (10)).

$$K_2O + CO_2 = K_2CO_3 \quad \Delta H_{300K} = -386 \text{ kJ mol}^{-1} \quad (8)$$

$$K_2O + 2CO_2 + H_2O = 2KHCO_3 \quad \Delta H_{300K} = -176 \text{ kJ mol}^{-1} \quad (9)$$

$$2KOH + CO_2 = K_2CO_3 + H_2O \quad \Delta H_{300K} = -154 \text{ kJ mol}^{-1} \quad (10)$$

$$KOH + CO_2 = KHCO_3 \quad \Delta H_{300K} = -156 \text{ kJ mol}^{-1} \quad (11)$$

In order to verify this, the analysis of the dynamics of surface species during an analogous CCR experiment is reported in Fig. 4A–D, in comparison with the reactor outlet gas stream concentrations (Fig. 4E). To optimise the temporal behaviour of the surface species analysis, the inlet flow condition for these experiments were set to 10 mL min^{-1} for the CO_2 feed (1% in He) and the H_2 feed, while the He flush was kept at 30 mL min^{-1}. The spectra are the average of 8 cycles after achieving a stable operation (quasi steady-state). The last spectrum of the cycle, collected at the end of the inert flushing phase, is used as the background to calculate the absorbance.

When CO_2 is fed to the catalyst bed (0–420 s), we observe the rise of specific vibrations in the CO stretching region (ν(CO) = 1640 and 1290 cm^{-1}). The outlet stream concentrations (Fig. 4E) clarify that those species are appearing on the surface before the rise of CO_2 signal at the outlet (*ca.* 200 s). When the saturation is reached at one position of the bed, the surface intermediates start forming at positions further in the bed. The delay observed at each position for the appearance of the ν(CO) stretching bands reproduces quite well the spatially-resolved profile of CO_2 along the catalytic bed obtained with *operando* gas sampling experiments (Fig. 3B). This confirms that those signals are directly related to the surface intermediates formed during CO_2 capture.

Such species were previously assigned to specific formates on potassium. Contrarily to what happens in H_2 + CO_2 cofeed

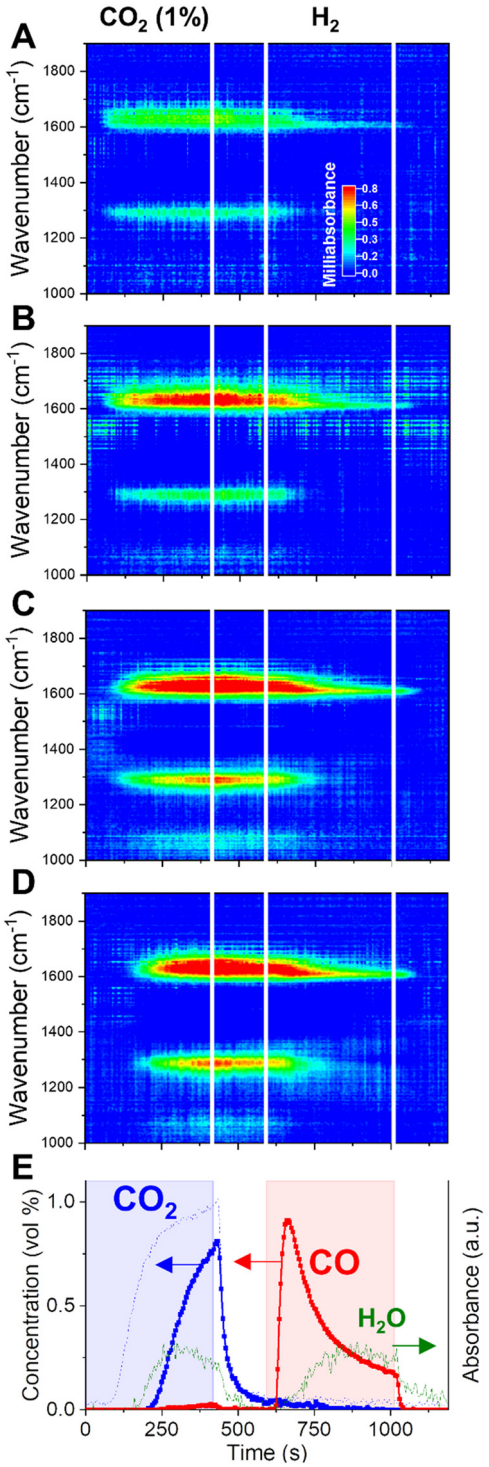

Fig. 4 Dynamic evolution of surface species elucidated by *operando* DRIFTS during CCR at 350 °C at different positions (A = 3.3 mm, B = 6.4 mm, C = 9.5 mm, D = 12.6 mm) of the catalyst bed from front (A) to back (D). Outlet gas composition (E) obtained by averaging 5 cycles at 350 °C. CO_2 blank signal (dotted line) obtained as average of 2 CCR cycles during a blank experiment at room temperature.

operation,[33] the rise of CH stretching bands (2700–2900 cm^{-1}) during the CO_2 capture is not observed here, indicating that formates may be not a stable intermediate for the

capture process. This is in line with the indication of low thermal stability of potassium formate species on Al_2O_3-supported catalysts, which would decompose to carbonates at temperature lower than 350 °C.[34,35] A similar consideration applies to eventual bicarbonate groups on potassium.[36] Rather, the absorption bands centered at 1640 and 1290 cm^{-1}, arising during CO_2 capture, reflect the splitting of the doubly degenerated asymmetric CO stretching vibration of carbonates, as a result of the lowered symmetry when coordinated to a surface metal cation. The high value of the splitting $\Delta\nu > 300$ cm^{-1}, reported for similar catalytic systems,[37,38] identifies the observed surface species as bidentate carbonates.[39,40] This represents a strong indication that the principal capture mechanism consists of the exothermic reaction of a KOH phase and CO_2 to form carbonates and water (reaction (10)). When the atmosphere is switched to inert flushing (at 420 s), neither a temperature change nor massive CO_x release is detected by spatial sampling (Fig. S4†), confirming a strong chemical interaction stabilising the adsorbed CO_x species on the catalyst surface. Nevertheless, a slight decrease in intensity of the DRIFTS bands is observed, indicating that the inert flushing may provoke only a limited removal of the surface intermediates formed during capture.

H_2 is essential to remove the surface species generated during CO_2 capture. Switching to H_2 flow (Fig. 3C), a sudden release of CO is detected instantaneously for each position along the catalytic bed. The removal of adsorbed CO_2 in the form of CO is a fast process. Spatiotemporal sampling of temperature during the reduction phase (Fig. 3E) indicates that the CO release is associated with only limited exothermicity and temporally confined at the beginning of the reduction phase. Such results confirm the absence of a redox cycle involving extensive copper oxidation, which would have in turn resulted in a highly exothermic reaction. Rather, H_2 is activated on the catalyst by dissociation on Cu and provokes the fast decomposition of the CO_2-derived surface intermediates.

In terms of surface species, it can be observed from the DRIFTS data in Fig. 4 that, at the switching to H_2 atmosphere (595 s), the bidentate carbonates formed during the capture phase are rapidly decomposed, as indicated by the fast decrease in the intensity of the corresponding ν(CO) stretching bands centered at 1640 and 1290 cm^{-1}. The fast removal of the surface intermediates for capture matches temporarily the fast release of CO detected in the outlet stream (Fig. 4E). Thus, a fast decomposition of the surface carbonates, induced by the presence of H_2, constitutes the principal route for the fast CO production in CCR and the regeneration of the active KOH phase (reaction (12)).

$$K_2CO_3 + H_2 = 2KOH + CO \quad (12)$$

After the fast release of CO, a long tailing of CO formation is observed. In DRIFTS, such tailing is associated with a narrow band in the CO stretching region centered around 1610 cm^{-1}. At the same time, IR absorption bands in the C–H stretching region appear at 2760 and 2670 cm^{-1} (Fig. S5†), at vibrational frequencies comparable with formates species on potassium.[41,42] Such bands indicate that, in presence of excess H_2, accumulation of formates on the surface may occur, which slowly decompose to CO and H_2O. In fact, formates were proposed as intermediates for CO formation in reverse-water gas shift catalysis, where CO_2 and H_2 are simultaneously fed.[43] However, in CCR conditions formate intermediates do not seem to be involved in the capture and fast reduction of captured CO_2. The slightly higher intensity of the formates bands for position towards the end of the bed (Fig. S5†) may indicate their accumulation due to limitations specific of the plug flow configuration, which can limit the efficient release of CO and the fast regeneration of the catalyst.

CO capture

To prove the participation of CO in the capture mechanism, we designed a CCR experiment in which the CO_2 phase is substituted by a diluted CO stream (0.5% in He) and performed *operando* DRIFTS. A direct comparison of dynamic surface species in presence of CO_2 or CO as reagents is aimed by employing the same catalyst bed of the experiment in Fig. 4 and analysing the position at 9.5 mm from the front end of the catalyst bed (the Fig. 4C position, the total bed length of 14 mm). The position was selected for providing

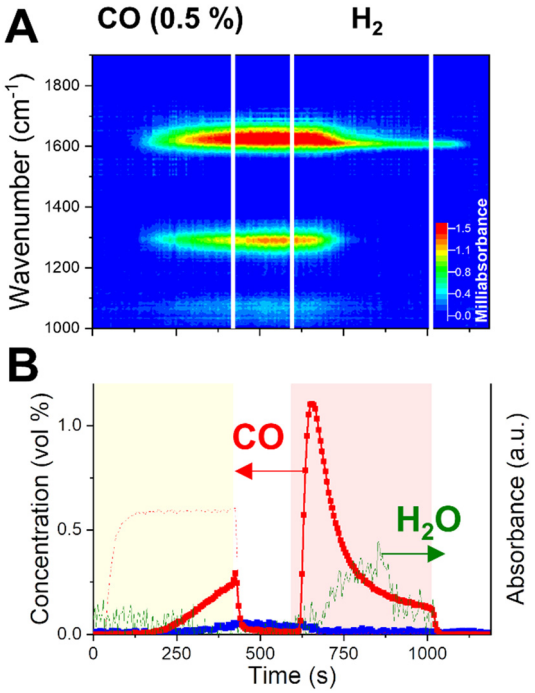

Fig. 5 Dynamic evolution of surface species elucidated by *operando* DRIFTS (A) during CO-CCR performed at 350 °C. Outlet gas composition (B) was obtained from averaging 5 cycles. CO blank signal (dotted line) obtained as average of 2 CCR cycles during a blank experiment at room temperature.

the best combination in terms of higher absorbance intensity and temporal resolution to discriminate the dynamic evolution of surface species, compared to positions at the front of the bed.

The results are reported in Fig. 5. When the inlet CO_2 is substituted by a CO stream, to our surprise, very similar catalytic behaviour and surface species dynamics are observed. During the capture phase (0–420 s), CO is effectively captured from the inlet stream. Such result indicates that the active sites on the catalyst surface, formed during the activation of potassium phase in H_2, have high affinity for both CO_2 and CO.

Fig. 5A reports the *operando* DRIFTS spectra obtained for one position towards the end of the catalyst bed. The CO capture is accompanied by the rise of the same absorption bands in the CO stretching region as observed during CO_2 capture (Fig. 4) and assigned to bidentate carbonates. At this position, such bands rise with a significant delay (*ca.* 200 s) with respect to the start of the CO feed, confirming the progress of a capture front along the bed until saturation of the active sites.

In contrast to the CO_2 capture (Fig. 4E), the absence of water release upon CO capture indicates a different type of interaction between CO and the catalytic surface. Alkali hydroxides such as NaOH and KOH are known to efficiently react with CO to form K_2CO_3 with release of H_2 (reaction (13)).[44,45]

$$2KOH + CO = K_2CO_3 + H_2 \quad (13)$$

Similarities to the CO_2-based CCR experiment are evidenced also in the reduction phase. When H_2 is sent to the reactor (595 s), a fast intense release of CO is detected at the outlet, associated with a drastic decrease in intensity of the surface carbonates bands. After that, a long tailing in the CO signal at the outlet is linked to the slow decay of a narrow band at 1610 cm^{-1}.

Simultaneously, the same bands appear in the ν(CH) stretching region (Fig. S6†) as observed in the CO_2-CCR experiment (Fig. S5†) and they are assigned to potassium formates species. However, contrary to the CO_2 experiment, the water signal rise is limited and drops before the end of the H_2 phase, implying the importance of extra oxygen atom in CO_2 for water formation.

CO_2 capture on oxidised catalytic surface

Previous *operando* XRD investigation by Hyakutake *et al.*[25] elucidated that, during CCR operation, a highly dispersed K phase is generated and strongly interacts with the metallic Cu, provoking its nanodispersion. The combination of dispersed potassium phase and metallic copper has been proven a critical property to induce the efficient CCR catalytic activity. Metallic Cu provides sites for H_2 dissociation and ensures the regeneration of the catalytically active phase by enhancing the decomposition of the potassium carbonate

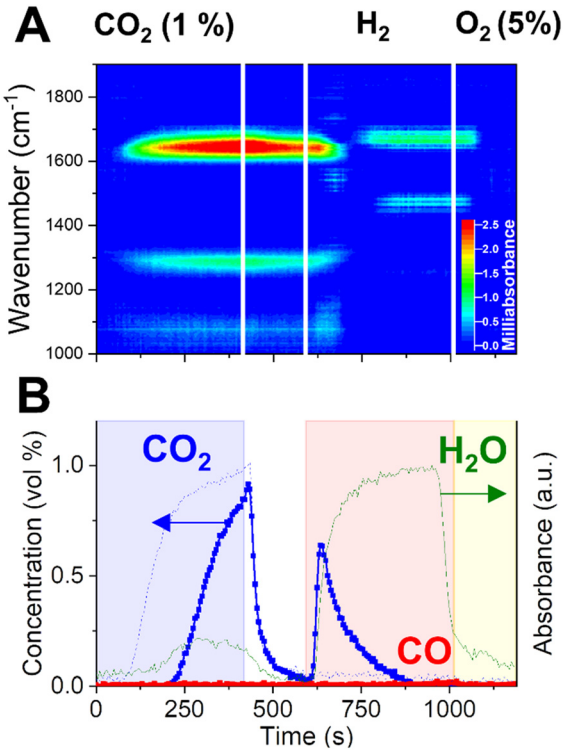

Fig. 6 Dynamic evolution of surface species elucidated by *operando* DRIFTS (A) during CCR performed at 350 °C with substitution of last He gas phase with O_2 (5% in He). Outlet gas composition (B) was obtained from averaging 5 cycles at 350 °C. CO_2 blank signal (dotted line) obtained as average of 2 CCR cycles during a blank experiment at room temperature.

phase. However, it is not clear whether Cu is playing a fundamental role in the CO_2 capture mechanism. To answer this, we performed a modified CCR experiment by introducing a diluted O_2 flow (5% in He) instead of the inert flushing phase of the end of each cycle. At the reaction temperature, it is expected that the introduction of oxygen in the reactor leads to the complete oxidation of the copper phase, while keeping intact the active potassium phase generated by decomposition of the potassium carbonate precursor in H_2. As a consequence, CO_2 capture takes place on a oxidised surface, which contains CuO.

Operando DRIFTS results obtained at a single position (9.5 mm in the bed, similar to Fig. 5A) are presented in Fig. 6A. Importantly, the capture of CO_2 is still observed in presence of an oxidised catalytic surface, as demonstrated by the delayed appearance of CO_2 at the reactor outlet. In terms of surface species, the typical CO stretching bands associated to bidentate carbonates are observed in the capture phase, apart for the band centered at 1650 cm^{-1}, whose peak presents a blue-shift compared to the experiments with CO_2 or CO capture on a reduced surface. This result may indicate a specific influence of metallic Cu in the bonding of carbonates species to the surface.

The amount of CO_2 captured and the evolution of the H_2O signal at the outlet are comparable to the ones observed in

the regular CCR experiment. In contrast, there is no CO detected when CO_2 interacts with an oxidised Cu surface. No modifications of the potassium phase are expected as a consequence of the oxygen treatment. The temperature of the reaction and the cyclic exposure to the highly reducing H_2 phase may not induce dehydration of KOH to K_2O, for which only limited evidences were reported.[46,47] The short O_2 treatment (175 s) employed in this experiment is not expected to specifically promote such phase transition. In agreement with the regular CCR operation, H_2O is detected during CO_2 capture and appears as a specific product of the capture reaction. KOH species are then expected to react with CO_2 to form potassium carbonates species observed on the surface and to release water (reaction (10)).

Furthermore, no detected CO in the capture phase indicates that the responsible reaction path is prohibited in presence of CuO. Since no evidences of extensive copper oxidation were found during regular CCR operation in this work and previous work, we are tempted to assign the CO formation in normal CCR to an hydrogenation reaction (reaction (2)), resulting from the interaction of CO_2 with specific H species activated on Cu. Such species may be oxidised during the forced Cu oxidation in the experiment shown in Fig. 6. Proof of this oxidation process is the water release observed at the reactor outlet during the O_2 flushing phase (1015–1190s).

Upon switching to H_2 (at 595 s), the presence of CuO activates its reduction accompanying significant production of water. Notably, no CO is released, and only removal of the captured species in the form of CO_2 is observed. The extensive release of water may destabilise the surface intermediate and promoting a water-gas shift type of reaction resulting in the removal of unconverted CO_2.

The most important observation is that the selective conversion of captured CO_2 to CO is lost in presence of oxidised Cu. *Operando* DRIFTS clarifies that, after the fast removal of surface carbonates and corresponding evolution of CO_2, new surface bands appear on the catalyst surface, which can be possibly assigned to adsorbed water due to high amount of water released from CuO reduction. However, it is proved that the Cu–K-based catalyst is able to efficiently capture CO_2 in presence of oxygen and water in the stream,[20] which is a functionality of interest for realistic application as the removal of CO_x species from flue gases in combustion and chemical plants.

Conclusions

This work investigated a Cu–K/Al_2O_3 catalyst with the aim of clarifying the principal reaction routes active in the CO_2 capture and its selective reduction to CO. The results indicate that the catalytically active phase for capture, first generated during activation in H_2 at 450 °C, may consist of highly dispersed KOH species. *Operando* sampling of gaseous concentration and temperature inside the catalyst bed revealed that, when the catalyst is exposed to CO_2 atmosphere, an exothermic reaction takes place progressively along the bed until saturation of the active site, accompanying a release of water. In addition, spatiotemporal *operando* DRIFTS confirmed that CO_2 is fixated on the catalyst surface in the form of bidentate carbonates species. During the CO_2 capture, the presence of metallic Cu and reactive hydrogen stored in the catalyst stimulates a CO_2 hydrogenation path to CO as side reaction. This side reaction takes place after completion of the active CO_2 capture period. By substituting CO_2 with CO in the feed, we demonstrated that CO can be also effectively captured by the catalyst material. However, this capture step does not involve the formation of water.

Switching the reactant feed to H_2, the regeneration of the catalyst and the selective release of CO take place. Combination of the spatiotemporal *operando* methodologies revealed that surface carbonates are rapidly decomposed, selectively generating CO and restoring the active phase for CO_2 capture. No water is released during the fast removal of surface carbonates, in agreement with a K_2CO_3 decomposition route and excluding the intervention of extensive copper oxidation in the reaction. After the initial fast release of CO, a tailing CO release is observed. This slow CO formation is caused by the decomposition of the surface formates formed on the potassium-containing species.

Intentionally oxidising the surface by O_2 before CO_2 capture, we proved that CO_2 capture can still take place in presence of CuO with formation of surface carbonates and release of water, reinforcing the hypothesis that the active phase for capture consists of KOH species. However, in the H_2 atmosphere, the excess water generated by CuO reduction leads to carbonates decomposition with release of unconverted CO_2. These insights have practical implications in designing better CCR catalysts and defining feed gas composition and operation conditions.

Experimental

Catalyst synthesis

Aluminum oxide (γ-phase, Thermo Fisher, catalyst support), was employed as support material. Cu and K were added by incipient wetness impregnation using copper nitrate trihydrate (Merck, >99.5%) and potassium carbonate anhydrous (Sigma, >99.0%) as precursors. Copper nitrate was first impregnated on the support, the resulting mixture was dried overnight at 80 °C and then calcined at 500 °C for 5 h. The obtained Cu/Al_2O_3 material was further impregnated with a K_2CO_3 aqueous solution to obtain the final composition (Cu/K/Al_2O_3, 11/10/79 wt%).

Catalyst characterization

Powder X-ray diffractograms were acquired on a Bruker D8 Advance Diffractometer with Bragg–Brentano geometry using monochromatic Co Kα radiation (λ = 1.7902 Å). BET surface area of the catalysts was determined from N_2 adsorption

isotherms at 77 K using a Micromeritics TriStar II 3020 instrument.

Catalytic testing

The reaction setup configuration was similar to the one described in previous works.[25] The gas controlling part consisted of mass flow controllers (MFCs, Bronkhorst) and two electric 4-way valves to switch among different gas flows at the inlets. After being pelletized, crushed and sieved in 200–300 μm range, 250 mg of catalyst material were placed in a tubular quartz tube reactor (4 mm ID, 6 mm OD). Blank experiments were conducted by passing the reaction gas mixture on the fresh, non-activated catalyst at room temperature. Prior to the catalytic experiment, the catalyst was activated by reduction under 50 mL min^{-1} of pure H_2 at 450 °C. The temperature of the bed was controlled by a thermocouple inserted in the quartz reactor. Catalytic performance was evaluated under CCR conditions at 350, 400 and 450 °C and ambient pressure. 15 mL min^{-1} of 9.9 vol% CO_2 in He, referred to as capture phase, was alternated to a reduction phase consisting of 15 mL min^{-1} of H_2 (100 vol%). An inert phase of He (30 mL min^{-1}, 100 vol%) was flushed between the capture and reducing phases (and *vice versa*). The effluent gas mixture composition was quantified by FT-IR spectroscopy (ALPHA Bruker) with a time resolution of 5 s. Valve switching and spectral acquisition were synchronized by LabView software. The data presented were obtained from the average of multiple cycles of operation, after a stable and reproducible composition of the effluent was achieved.

Spatiotemporal sampling of temperature and gas composition

For the spatiotemporal analysis of temperature and gas composition along the catalyst bed, the reaction setup was modified introducing a stainless steel capillary in the reactor through the centre of the packed bed. The capillary (inner diameter = 500 μm, outer diameter = 700 μm, REACNOSTICS GmbH) had 4 holes for gas sampling, equally distanced at the same axial position, with diameter of 50 μm. For measuring the temperature at the sampling position, a thermocouple was inserted through the capillary, with the tip aligned with the sampling holes. The capillary end was sealed with epoxy glue, fixing the thermocouple in place. The other end of the capillary was connected to a mass spectrometer (Omnistar Pfeiffer Vacuum). The reactor effluent was analysed by the FT-IR as explained previously. The same experimental conditions employed for the catalytic testing were applied.

Operando DRIFTS

The DRIFTS measurements were carried out in a custom-made reaction cell, similar to a previously reported design,[48] mounted in a Harrick praying mantis optical system. The reaction cell consisted of a 2 × 2 mm rectangular channel, sealed with a ZnSe window on the top, which limited the operation temperature to 350 °C. A catalyst pellet mass of 160 mg was tested, which translated to a bed length in the reaction cell of *ca.* 14 mm. Acquiring DRIFT spectra at different positions on the catalytic bed was possible by moving the entire reactor cell, mounted on an actuator. Prior to the reaction, the catalyst was reduced at 350 °C for 1 h in H_2 (30 mL min^{-1}, 100 vol%). For the regular CCR experiments, CO_2 (10 mL min^{-1}, 1 vol% in He, 420 s), He (30 mL min^{-1}, 100 vol%, 175 s) and H_2 (10 mL min^{-1}, 100 vol%, 420 s) and He (30 mL min^{-1}, 100 vol%, 175 s) phases were alternatingly passed to the reactor. CO (10 mL min^{-1}, 0.5 vol% in He, 420 s) and O_2 (30 mL min^{-1}, 5 vol% in He, 175 s) phases were also employed in dedicated experiments. Spectra were acquired using a Bruker INVENIO R FT-IR spectrometer, equipped with a liquid-nitrogen-cooled MCT detector. Before measurements, a background was taken over the completely reduced catalyst. DRIFT spectra were averaged over consecutive, reproducible cycles to improve signal to noise ratio (S/N). The reactor effluent was analysed by means of FT-IR spectroscopy as explained previously.

Conflicts of interest

There are no conflicts to declare.

References

1 M. Peters, B. Köhler, W. Kuckshinrichs, W. Leitner, P. Markewitz and T. E. Müller, *ChemSusChem*, 2011, **4**, 1216–1240.
2 C. J. Quarton and S. Samsatli, *Appl. Energy*, 2020, **257**, 113936.
3 M. Aresta, A. Dibenedetto and A. Angelini, *Chem. Rev.*, 2014, **114**, 1709–1742.
4 A. Otto, T. Grube, S. Schiebahn and D. Stolten, *Energy Environ. Sci.*, 2015, **8**, 3283–3297.
5 M. Bui, C. S. Adjiman, A. Bardow, E. J. Anthony, A. Boston, S. Brown, P. S. Fennell, S. Fuss, A. Galindo, L. A. Hackett, J. P. Hallett, H. J. Herzog, G. Jackson, J. Kemper, S. Krevor, G. C. Maitland, M. Matuszewski, I. S. Metcalfe, C. Petit, G. Puxty, J. Reimer, D. M. Reiner, E. S. Rubin, S. A. Scott, N. Shah, B. Smit, J. P. M. Trusler, P. Webley, J. Wilcox and N. Mac Dowell, *Energy Environ. Sci.*, 2018, **11**, 1062–1176.
6 M. Ramdin, T. W. de Loos and T. J. H. Vlugt, *Ind. Eng. Chem. Res.*, 2012, **51**, 8149–8177.
7 W. Gao, S. Liang, R. Wang, Q. Jiang, Y. Zhang, Q. Zheng, B. Xie, C. Y. Toe, X. Zhu, J. Wang, L. Huang, Y. Gao, Z. Wang, C. Jo, Q. Wang, L. Wang, Y. Liu, B. Louis, J. Scott, A.-C. Roger, R. Amal, H. He and S.-E. Park, *Chem. Soc. Rev.*, 2020, **49**, 8584–8686.
8 S.-i. Nakao, K. Yogo, K. Goto, T. Kai and H. Yamada, *Advanced CO_2 capture technologies: absorption, adsorption, and membrane separation methods*, Springer, 2019.
9 P. Markewitz, W. Kuckshinrichs, W. Leitner, J. Linssen, P. Zapp, R. Bongartz, A. Schreiber and T. E. Müller, *Energy Environ. Sci.*, 2012, **5**, 7281–7305.

10 J. Wang, L. Huang, R. Yang, Z. Zhang, J. Wu, Y. Gao, Q. Wang, D. O'Hare and Z. Zhong, *Energy Environ. Sci.*, 2014, **7**, 3478–3518.
11 Y. Belmabkhout, V. Guillerm and M. Eddaoudi, *Chem. Eng. J.*, 2016, **296**, 386–397.
12 L.-C. Lin, A. H. Berger, R. L. Martin, J. Kim, J. A. Swisher, K. Jariwala, C. H. Rycroft, A. S. Bhown, M. W. Deem, M. Haranczyk and B. Smit, *Nat. Mater.*, 2012, **11**, 633–641.
13 J. Blamey, E. J. Anthony, J. Wang and P. S. Fennell, *Prog. Energy Combust. Sci.*, 2010, **36**, 260–279.
14 IEA, *CCUS in Clean Energy Transitions*, International Energy Agency, Paris, 2020.
15 M. Mikkelsen, M. Jørgensen and F. C. Krebs, *Energy Environ. Sci.*, 2010, **3**, 43–81.
16 H.-J. Ho, A. Iizuka and E. Shibata, *Ind. Eng. Chem. Res.*, 2019, **58**, 8941–8954.
17 P. Melo Bravo and D. P. Debecker, *Waste Dispos. Sustain. Energy*, 2019, **1**, 53–65.
18 I. S. Omodolor, H. O. Otor, J. A. Andonegui, B. J. Allen and A. C. Alba-Rubio, *Ind. Eng. Chem. Res.*, 2020, **59**, 17612–17631.
19 M. S. Duyar, M. A. A. Treviño and R. J. Farrauto, *Appl. Catal., B*, 2015, **168–169**, 370–376.
20 L. F. Bobadilla, J. M. Riesco-García, G. Penelás-Pérez and A. Urakawa, *J. CO2 Util.*, 2016, **14**, 106–111.
21 S. Cimino, F. Boccia and L. Lisi, *J. CO2 Util.*, 2020, **37**, 195–203.
22 E. L. G. Oliveira, C. A. Grande and A. E. Rodrigues, *Sep. Purif. Technol.*, 2008, **62**, 137–147.
23 A. Porta, R. Matarrese, C. G. Visconti, L. Castoldi and L. Lietti, *Ind. Eng. Chem. Res.*, 2021, **60**, 6706–6718.
24 H. Sun, J. Wang, J. Zhao, B. Shen, J. Shi, J. Huang and C. Wu, *Appl. Catal., B*, 2019, **244**, 63–75.
25 T. Hyakutake, W. van Beek and A. Urakawa, *J. Mater. Chem. A*, 2016, **4**, 6878–6885.
26 L. Proaño, E. Tello, M. A. Arellano-Trevino, S. Wang, R. J. Farrauto and M. Cobo, *Appl. Surf. Sci.*, 2019, **479**, 25–30.
27 A. Porta, C. G. Visconti, L. Castoldi, R. Matarrese, C. Jeong-Potter, R. Farrauto and L. Lietti, *Appl. Catal., B*, 2021, **283**, 119654.
28 A. Bermejo-López, B. Pereda-Ayo, J. A. González-Marcos and J. R. González-Velasco, *J. CO2 Util.*, 2019, **34**, 576–587.
29 L. Hu and A. Urakawa, *J. CO2 Util.*, 2018, **25**, 323–329.
30 F. Kosaka, Y. Liu, S.-Y. Chen, T. Mochizuki, H. Takagi, A. Urakawa and K. Kuramoto, *ACS Sustainable Chem. Eng.*, 2021, **9**, 3452–3463.
31 Y. A. Daza and J. N. Kuhn, *RSC Adv.*, 2016, **6**, 49675–49691.
32 Y. Duan, D. R. Luebke and H. H. Pennline, *Int. J. Clean Coal Energy*, 2012, **1**, 1–11.
33 A. Bansode, B. Tidona, P. R. von Rohr and A. Urakawa, *Catal. Sci. Technol.*, 2013, **3**, 767–778.
34 K. Kobl, L. Angelo, Y. Zimmermann, S. Sall, K. Parkhomenko and A.-C. Roger, *C. R. Chim.*, 2015, **18**, 302–314.
35 P. Baraldi, *Spectrochim. Acta, Part A*, 1979, **35**, 1003–1007.
36 M. Hartman, K. Svoboda, B. Čech, M. Pohořelý and M. Šyc, *Ind. Eng. Chem. Res.*, 2019, **58**, 2868–2881.
37 K. Coenen, F. Gallucci, B. Mezari, E. Hensen and M. van Sint Annaland, *J. CO2 Util.*, 2018, **24**, 228–239.
38 N. D. Parkyns, *J. Chem. Soc. A*, 1969, 410–417.
39 G. Busca and V. Lorenzelli, *Mater. Chem.*, 1982, **7**, 89–126.
40 G. J. Millar, C. H. Rochester and K. C. Waugh, *J. Chem. Soc., Faraday Trans.*, 1992, **88**, 1477–1488.
41 G. J. Millar, C. H. Rochester and K. C. Waugh, *J. Catal.*, 1995, **155**, 52–58.
42 I. L. C. Freriks, P. C. de Jong-Versloot, A. G. T. G. Kortbeek and J. P. van den Berg, *J. Chem. Soc., Chem. Commun.*, 1986, 253–255.
43 C.-S. Chen, W.-H. Cheng and S.-S. Lin, *Catal. Lett.*, 2000, **68**, 45–48.
44 M. C. Boswell and J. V. Dickson, *J. Am. Chem. Soc.*, 1918, **40**, 1779–1786.
45 S. Kumar, V. Drozd and S. K. Saxena, *Catalysts*, 2012, **2**, 532–543.
46 C. Di Blasi, A. Galgano and C. Branca, *Energy Fuels*, 2009, **23**, 1045–1054.
47 T. Otowa, R. Tanibata and M. Itoh, *Gas Sep. Purif.*, 1993, **7**, 241–245.
48 A. Urakawa, N. Maeda and A. Baiker, *Angew. Chem., Int. Ed.*, 2008, **47**, 9256–9259.